Rare Met. (2024) 43(2):522–532
https://doi.org/10.1007/s12598-023-02425-7

RARE METALS

ORIGINAL ARTICLE

Synergistically coupling of Ni–Fe LDH arrays with hollow Co–Mo sulfide nanotriangles for highly efficient overall water splitting

Yun Jae Lee, Seung-Keun Park*

Received: 23 February 2023 / Revised: 13 April 2023 / Accepted: 21 April 2023 / Published online: 14 November 2023

Abstract Developing bifunctional catalysts that can catalyze both oxygen evolution reaction (OER) and hydrogen evolution reaction (HER) is pivotal to commercializing large-scale water splitting. Herein, a novel hollow nanotriangle composed of NiFe LDH-$CoMoS_x$ heterojunction (H-CMS_x@NiFe LDH) is proposed as a highly efficient bifunctional electrocatalyst for both OER and HER. To fabricate a heterojunction system, ultra-thin nickel–iron layered double hydroxide (NiFe LDH) nanosheets are uniformly electrodeposited onto a metal–organic framework-derived hollow $CoMoS_x$ nanotriangle. The strong coupling of $CoMoS_x$ and NiFe LDH catalysts forms the intimate heterojunction interfaces to facilitate interfacial charge transfer, which is favorable to enhance the bifunctional catalytic activity. Moreover, the large void of $CoMoS_x$ nanotriangles and interconnected ultra-thin NiFe LDH nanosheets result in good electrolyte penetration and gas release. Therefore, the as-prepared H-CMS_x@NiFe LDH on nickel foam (NF) exhibits an impressive catalytic activity and durability for OER and HER activities, delivering a current density of 100 $mA{\cdot}cm^{-2}$ at the small overpotentials of 214 and 299 mV in OER and HER, respectively. Meanwhile, H-CMS_x@NiFe LDH/NF proves to be an effective electrode for an alkaline electrolyzer, as a voltage of only 1.99 V is enough to achieve a current density voltage of only 1.99 V is enough to achieve a current density of 400 $mA{\cdot}cm^{-2}$ with no degradation in performance over 50 h.

Keywords Overall water splitting; Metal–organic framework; Molybdenum sulfide; Layered double hydroxide; Heterojunction

1 Introduction

Electrocatalytic water splitting is an ideal technique for the sustainable and clean production of H_2. This technique uses an anodic oxygen evolution reaction (OER) and a cathodic hydrogen evolution reaction (HER) [1–4]. Conventionally, precious metal Pt-based catalysts are used for HER, and Ir- and Ru-based catalysts are used for OER; however, their expensive price and scarcity hinder the commercialization of large-scale water splitting [5–9]. Motivated by these challenges, significant research efforts have been devoted to developing a relatively inexpensive electrocatalyst with high electrocatalytic activity, especially for both reactions.

Molybdenum sulfide (MoS_x)-based nanostructures have been studied intensively as promising non-precious electrocatalysts, due to their various advantages such as low price, high electrochemical activity, and excellent chemical stability [10, 11]. Recently, several studies have reported that incorporating certain cations such as Co^{2+}, Fe^{2+}, and Ni^{2+} into the MoS_x nanostructure can significantly enhance

Supplementary Information The online version contains supplementary material available at https://doi.org/10.1007/s12598-023-02425-7.

Y. J. Lee, S.-K. Park*
Department of Advanced Materials Engineering, Chung-Ang University, Anseong, Gyeonggi-do 17546, Republic of Korea
e-mail: skpark09@cau.ac.kr

S.-K. Park
Department of Intelligent Energy and Industry, Chung-Ang University, 84 Heukseok-ro Dongjak-gu, Seoul 06974, Republic of Korea

S.-K. Park
Western Seoul Center, Korea Basic Science Institute, 150 Bugahyeon-ro, Seodaemun-gu, Seoul 03759, Republic of Korea

the electrochemical activity of MoS_x over the entire pH range by regulating the energy barrier [12–14]. However, unfortunately, most reported MoS_x-based catalysts only showed satisfactory activity toward HER, indicating the need for further catalyst development for OER, which is a major factor complicating the fabrication of an integrated water electrolyzer [15–19]. Therefore, it is urgent to develop MoS_x-based catalysts with high electrocatalytic activity for HER and for OER to simplify the fabrication process of the electrolyzer and reduce the production cost for commercializing large-scale water splitting. In this regard, the construction of a hetero-nanostructure by coupling the MoS_x-based catalysts with OER-active catalysts can be a feasible strategy to achieve a highly efficient bifunctional catalyst for water electrolysis.

For OER, nickel–iron-based layered double hydroxide (NiFe LDH) exhibits superior electrocatalytic performance under an alkaline condition due to its optimal electronic configuration and kinetic energy for the reaction [20–22]. Nevertheless, as is the case with most LDH materials, NiFe LDHs still suffer from poor stability and reduced electrochemical surface area caused by self-aggregation during the OER as well as relatively unsatisfactory HER activity [23–26]. To overcome these limitations, an electrodeposition method for directly growing NiFe LDH on substrates with a large surface area has been proposed recently, which improves the electrocatalytic activity of NiFe LDH by increasing the active sites [27, 28]. Moreover, the strong coupling can form intimate heterojunction interfaces between NiFe LDH and the substrates, which can modify the local charge distribution for achieving high electrocatalytic activities [29, 30]. Considering previous studies, the electrochemical coupling of NiFe LDHs with heteroatom incorporated MoS_x nanostructures can be an effective strategy to compensate for the limitations of each component's catalytic properties toward HER or OER.

Accordingly, herein, we fabricated a novel hollow nanotriangle composed of NiFe LDH- $CoMoS_x$ heterojunction (H-CMS_x@NiFe LDH) as a bifunctional electrocatalyst for both OER and HER. Co-based zeolitic imidazolate (ZIF-67)-derived hollow $CoMoS_x$ nanotriangles serve as the substrate for the uniform growth of ultrathin NiFe LDH nanosheets during the electrodeposition process. The strong coupling of $CoMoS_x$ and NiFe LDH catalysts forms intimate heterojunction interfaces to facilitate interfacial charge transfer, which enhances the bifunctional catalytic activity. Beyond that, a large void of $CoMoS_x$ nanotriangles and interconnected ultra-thin NiFe LDH nanosheets contribute to good gas release and electrolyte penetration. As expected, the as-prepared H-CMS_x@NiFe LDH on nickel foam (NF) exhibits outstanding catalytic performances toward OER and HER activities and durability; small overpotentials of 214 and 299 mV at a current density of 100 $mA{\cdot}cm^{-2}$ in OER and HER, respectively. Moreover, an alkaline electrolyzer using H-$CoMoS_x$@NiFe LDH/NF as both cathode and anode requires only low voltage of 1.99 V to achieve a current density of 400 $mA{\cdot}cm^{-2}$, and the overpotential remains stable with no significant change, even after 50-h continuous operation at 50 $mA{\cdot}cm^{-2}$.

2 Experimental

2.1 Preparation H-CMS_x/NF and H-CoS_x/NF

To obtain the the immersion solution, aqueous solution A and B, containing 16 mmol 2-methylimidazole (2-MIM) and 2 mmol $Co(NO)_3$ $6H_2O$, respectively, were mixed evenly with each other. The cleaned NF were completely immersed in the prepared mixture solution for 4 h to grow the ZIF-67 nanotriangles on the surface of NF (ZIF-67/NF). After the vacuum drying, ZIF-67/NF was treated in the DI/ethanol (1:6 in volume ratio) solution with 30 mg ammonium tetrathiomolybdate (ATTM) for 2 h at room temperature. The resultant product was rinsed and performed vacuum drying. As a comparison, H-CoS_x/NF was prepared by the chemical reaction between thioacetamide (TAA, 0.4 g) and ZIF-67/NF in ethanol solution.

2.2 Preparation of H-CMS_x@NiFe LDH/NF and NiFe LDH/NF

The NiFe LDH nanosheets were uniformly grown on the H-CMS_x/NF and bare NF substrates by the electrodeposition method in a typical 3-electrode system using saturated calomel electrode (SCE) and Pt wire as the reference and counter electrodes (RE and CE), respectively. Electrodeposition was carried out in the electrolyte solution containing nickel nitrate hexahydrate (15 $mmol{\cdot}L^{-1}$) and iron sulfate heptahydrate (15 $mmol{\cdot}L^{-1}$) at a steady voltage of − 1.0 V (vs. SCE) for 60 s. The loading mass of H-CMS_x@NiFe LDH/NF was measured to be 4.5 $mg{\cdot}cm^{-2}$. As compared, NiFe LDH/NF was obtained by the direct electrodeposition on the NF under the same conditions.

2.3 Materials characterization

The morphology and structure of the sample was analyzed by field-emission scanning electron microscopy (FESEM, HITACHI S-4300, operated at 15 kV) and high-resolution

transmission electron microscopy (HRTEM, JEOL-2100F, Korea Basic Science Institute, Busan, operated at 200 kV). The crystallinity of the sample was measured from 20° to 80° at 2 (°)·min^{-1} using X-ray diffraction (XRD) with Cu Kα radiation (0.15406 nm) at 40 kV. X-ray photoelectron spectroscopy (XPS, K-Alpha^{+}, Thermo Fisher Scientific) was used to analyze the oxidation state of the composite, in which Al Kα (1486.6 eV) was used with a constant powder of 100 W. The binding energies were calibrated based on the position of C 1s (284.6 eV).

2.4 Electrochemical measurement

The electrochemical measurements were carried out using a 3-electrode system with a ZIVE-SP1 instrument (WonA Tech Corp., Korea). The working electrode was prepared by loading the catalyst on a 1 cm × 1 cm NF. The Hg/HgO and Pt wire (or carbon rod in OER) and were used as the reference electrode and counter electrode, respectively. A KOH solution (1.0 mol·L^{-1}) was used as the electrolyte. For electrodeposition, an SCE was used as the RE. The linear sweep voltammetry (LSV) analysis was performed from 0.2326 to 0.6326 and − 0.8674 to − 1.2674 V versus Hg/HgO at a scan rate of 2 mV·s^{-1} in the OER and HER processes, respectively. All LSV curves were calibrated with *iR*-compensation by this equation: $E = E_{RHE} - iR_s$, where E is the *iR*-corrected potential, E_{RHE} is the measured potential with respect to RHE, i is the measured current R_s is the uncompensated resistance as determined by EIS. The durability of the catalyst was evaluated at current density of 50 mA·cm^{-2} using chronopotentiometry in the OER, HER, and overall water splitting process, respectively. The electrochemical surface areas (ECSAs) obtained by cyclic voltammetry (CV) were measured at 0.2–0.3 V versus a reversible hydrogen electrode (*vs.* RHE) at different scan rates. Electrochemical impedance spectroscopy (EIS) was performed in the frequency range of 0.1 Hz to 100 kHz. To convert the measured potential to RHE, the equation $E_{RHE} = E_{Hg/HgO} + 0.0591 \times pH + 0.14$ was used, where $E_{Hg/HgO}$ is measured potential using Hg/HgO electrode. Faradaic efficiency (FE) was calculated using the following equation: FE = V_g (experimental)/V_g (theoretical), where V_g (experimental) is the measured volume of gas, and the formula V_g(theoretical) = $[(i \times t)/(n \times F)] \times 24.5$ L·mol^{-1} is used, where i is the current, t is time, n is the number of electron moles, and F is the Faraday constant (96,485 C·mol^{-1}). As the comparison electrodes, the Pt-C 20 wt% and RuO_2 were loaded onto the Nickel foam (NF, 0.25 mg·cm^{-2} each). Briefly, a catalyst ink was made by combining 5 mg catalyst powder with a solution of 950 µl isopropyl alcohol and deionized water, and 50 µl Nafion, then sonicating for 0.5 h. 50 µl catalyst ink was added drop-wise to NF to produce the Pt-C/NF and RuO_2/NF samples.

3 Results and discussion

3.1 Synthesis of characterization of H-CoS_x/NF, H-CMS_x/NF, NiFe LDH/NF and H-CMS_x@NiFe LDH/NF

As illustrated in Scheme 1, a hierarchical heterostructured H-CMS_x@NiFe LDH nanoarray was prepared by a three-step process. First, ZIF-67 was grown on NF through a simple reaction between $Co(NO_3)\cdot 6H_2O$ and 2-MIM in deionized (DI) water. Scanning electron microscopy (SEM) image (Fig. 1a, e) shows that triangular-shaped ZIF-67 with a smooth surface is uniformly and densely deposited on NF (Scheme 1-①). In the second step, triangular-shaped hollow CMS_x was fabricated through an anion exchange reaction with ATTM followed by a post-annealing treatment (Scheme 1-②), according to a previously reported paper [12, 31, 32]. The ZIF-67 precursor partially dissolves in DI water and releases Co ions, which can easily react with the thiomolybdate anion (MoS_4^{2-}) generated from ATTM. The spontaneous reaction between Co ions and MoS_4^{2-} can form an insoluble $CoMoS_x$ solid around the surface of the precursor due to the difference in their diffusion rates, generating a large inner void within a triangular structure. The inner void can be distinctly identified from some triangles with a broken outer shell (Fig. 1b, f). The transformation of ZIF-67 into $CoMoS_x$ was also visually confirmed through the color change of the sample from pale purple to black (Fig. S1). Finally, NiFe LDH nanosheets were successfully grown on the surface of H-CMS_x/NF by the electrodeposition technique (Scheme 1-③), as shown in SEM images (Fig. 1c, g). Notably, compared to NiFe LDH directly grown on NF (Fig. 1d, h), NiFe LDHs on hollow CMS_x nanotriangles have significantly reduced lateral size and thickness, resulting in denser deposition of NiFe LDH nanosheets on the nanotriangles. Moreover, it was confirmed that the NiFe LDH nanosheets were cleanly deposited without aggregations only on the surface of hollow CMS_x nanotriangles, suggesting that hollow CMS_x nanotriangles can provide more nucleation sites for the growth of NiFe LDH.

To reveal the detailed structures of H-CMS_x and H-CMS_x@NiFe LDH, transmission electron microscopy (TEM) analysis was conducted (Fig. 2). From TEM images of both samples, a unique hollow structure of nanotriangles was identified by the distinct contrast between the inner body and outer shells (Fig. 2a, e). For H-CMS_x@NiFe LDH, the NiFe LDH nanosheets with a lamellar structure were visible on the surface of nanotriangles, and they have a length of approximately 186 nm (Fig. 2f). In the high-resolution TEM (HRTEM) image (Fig. 2c) of H-CMS_x, no distinct crystalline lattice correlated to the crystal structure

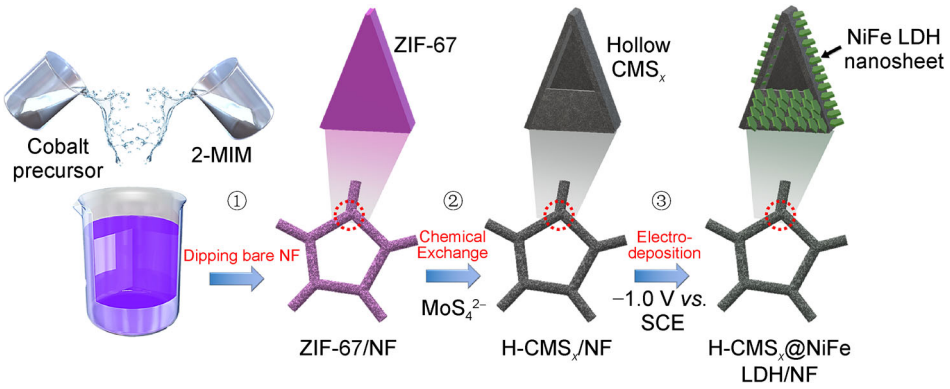

Scheme 1 Schematic illustration of fabrication procedures for H-CMS$_x$@NiFe LDH/NF electrode

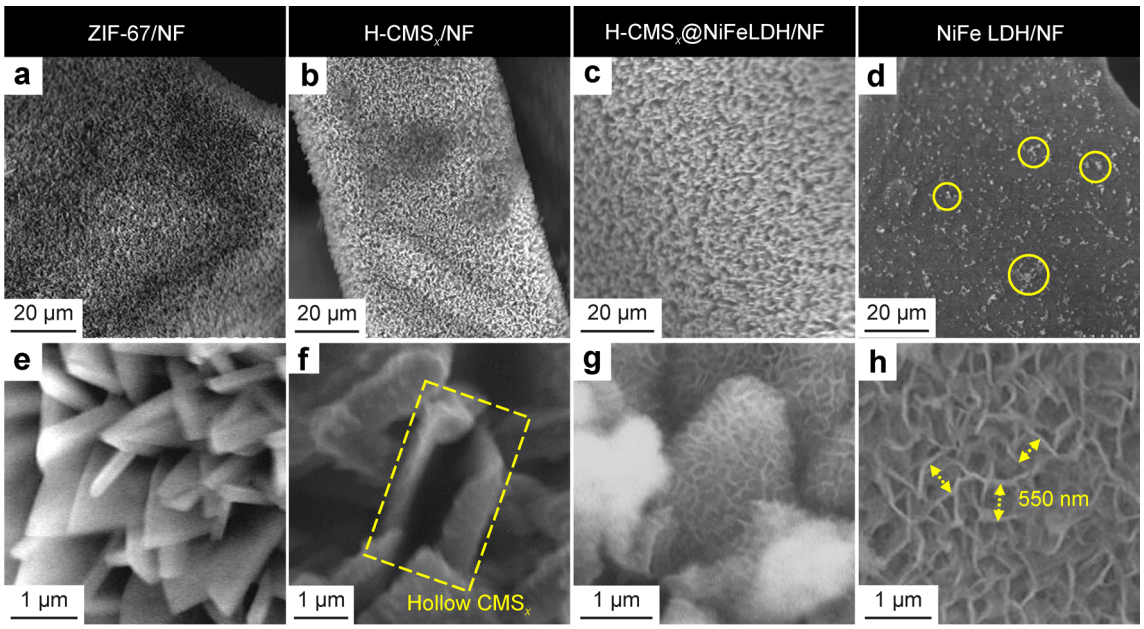

Fig. 1 SEM images of **a, e** ZIF-67/NF, **b, f** H-CMS$_x$/NF, **c, g** H-CMS$_x$@NiFe LDH/NF and **d, h** NiFe LDH/NF electrodes

of CoMoS$_x$ was found. Moreover, XRD pattern (Fig. S2) of H-CMS$_x$ and H-CMS$_x$@NiFe LDH exhibited only peaks related to metallic NF due to the small amount of active material deposited. After adjusting the intensity range (Fig. S3), XRD pattern of the H-CMS$_x$@NiFe LDH (Fig. S3) showed mostly very weak peaks at 34.6°, 39.0°, 60.3°, and 65.2°, which identified as crystal planes of NiFe LDH (JCPDS No. 51–0463). HRTEM image (Fig. 2g) of H-CMS$_x$@NiFe LDH confirmed well-aligned crystalline planes separated by 0.22 nm, corresponding to the (010) plane for NiFe LDH nanosheets [33, 34]. Similarly, in the selected area electron diffraction (SAED), only (010), (012), and (110) planes of NiFe LDH were identified (inset in Fig. 2g). In energy dispersive X-ray (EDX) mapping, Co, Mo, S, Ni and Fe were detected (Fig. 2h). In addition, more Co and S were detected in the shell region of H-CMS$_x$@NiFe LDH due to the hollow structure of CMS$_x$ nanotriangles. Meanwhile, the uniformly distributed Ni and Fe suggests the homogeneous deposition of NiFe LDH on H-CMS$_x$ nanotriangles. From EDX quantitative analysis result, the atomic ratio of Co, Mo, and S was determined as 0.8:0.2:1.0; thus, the chemical formula of CMS$_x$ is $(Co_{0.8}Mo_{0.2})S$. The ratio of Ni and Fe was calculated to be about 3:1 (Fig. S4), which is consistent with those of the reported NiFe LDHs [35, 36].

XPS measurement was performed on NiFe LDH, $_x$, and $_x$@NiFe LDH to confirm the electronic states of components (Fig. 3). All samples were prepared by deposition on a carbon cloth substrate to accurately measure the electronic state of Ni. The survey spectrum of $_x$@NiFe LDH (Fig. S5) showed the presence of Co, Mo, S, Ni, and Fe elements. In the HR Co 2p spectra of $_x$, three distinct doublets can be confirmed, with Co $2p_{3/2}$ binding energies at 778.9, 781.3 and 785.9 eV. The sharp peak located at

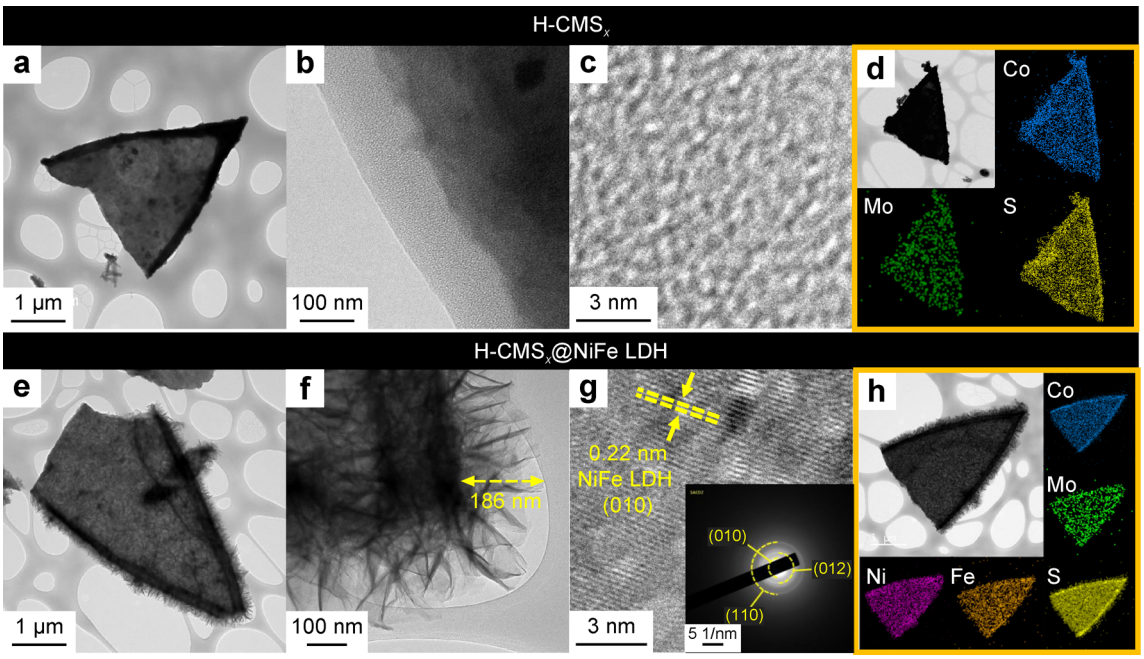

Fig. 2 TEM analysis results of **a-d** H-CMS$_x$ and **e–h** $_x$@NiFe LDH

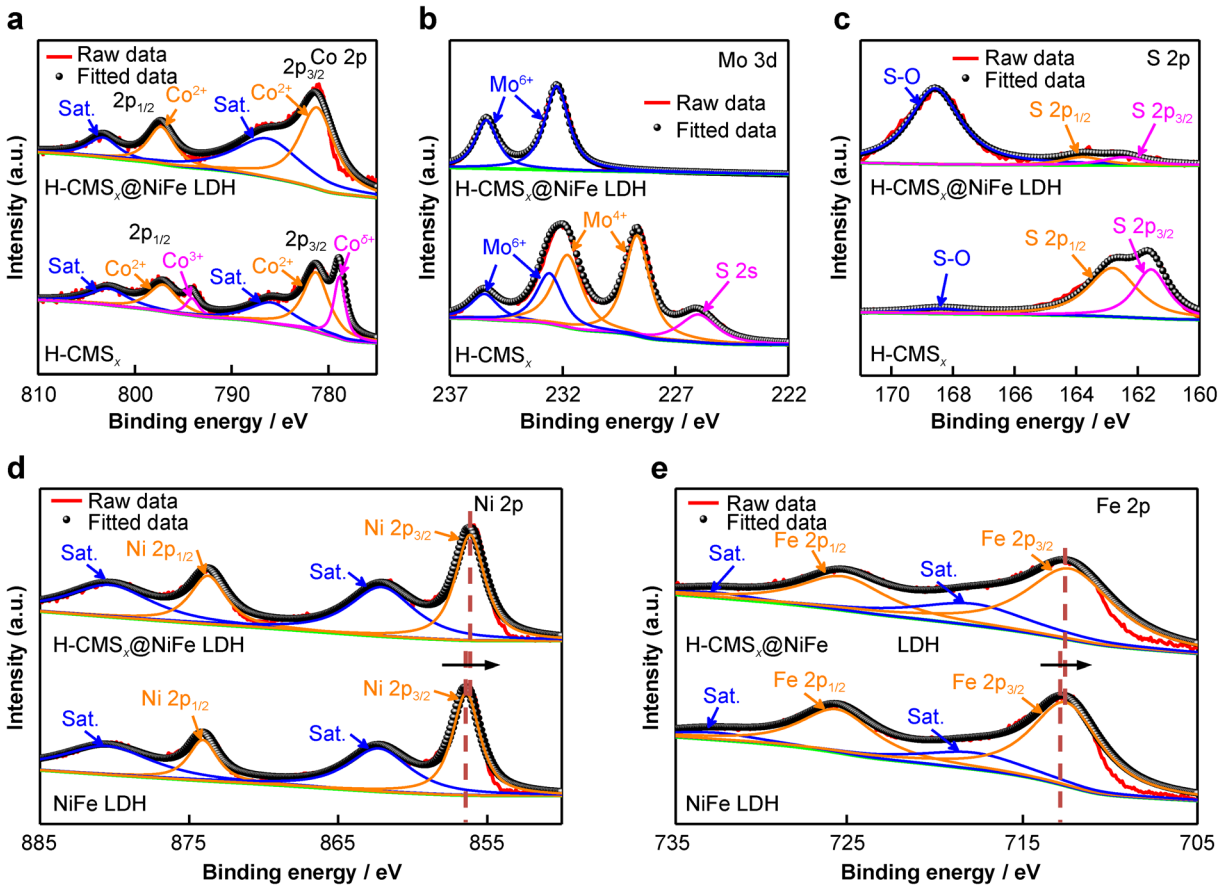

Fig. 3 High-resolution XPS spectra of H-CMS$_x$, NiFe LDH and H-CMS$_x$@NiFe LDH electrodes: **a** Co 2p, **b** Mo 3d, **c** S 2p, **d** Ni 2p and **e** Fe 2p

778.9 eV is attributed to reduced Co species ($Co^{\delta+}$, $0 < \delta < 2$) [37]. Notably, this peak almost disappeared after the deposition of NiFe LDH nanosheets, indicating the partial oxidation of Co species. Similarly, in HR Mo 3d and S 2p spectra of $_x$@NiFe LDH, it was verified that both Mo and S species were oxidized after combining $_x$ with NiFe LDH nanosheets (Fig. 3b, c); the intensity of peaks related to Mo^{6+} and S–O significantly increased, while that of other peaks decreased. The Ni and Fe 2p spectra of NiFe LDH and $_x$@NiFe LDH (Fig. 3d, e) showed two main peaks corresponding to Ni $2p_{3/2}$/Ni $2p_{1/2}$ and Fe $2p_{3/2}$/Fe $2p_{1/2}$ along with satellite peaks attributed to the presence of NiFe LDH nanosheets. Notably, the binding energies of Ni 2p and Fe 2p for H-CMS$_x$@NiFe LDH were negatively shifted compared with those of NiFe LDH, indicating the partial reduction of Ni and Fe species [27]. These results prove the formation of a strongly coupled heterojunction between H-CMS$_x$ and NiFe LDH, which can modify the local charge distribution for high electrocatalytic activities [38].

3.2 Investigation of catalytic properties for OER, HER, and water splitting

The electrocatalytic performances of the prepared catalysts were measured using a standard 3-electrode system in 1.0 mol·L^{-1} KOH electrolyte. Figure 4a shows the linear sweep voltammetry (LSV) curves of various catalysts for the OER process. Compared to bare NF, all catalysts exhibited a significantly improved electrocatalytic activity. It was observed that the oxidation peak in the LSV curve at 1.4 V corresponded to the oxidation of Ni(II)/Ni(III) species [39, 40]. Considering this fact, the larger oxidation peak of H-CMS$_x$@NiFe LDH/NF compared to other samples can be due to the presence of a higher number of active sites. [41]. Thus, the potential at 10 mA·cm^{-2} was not directly readable from LSV curve, we estimated it by extrapolating the curve (Fig. S6) [42]. As shown in Fig. 4b, the required overpotentials of H-CMS$_x$/NF were lower than those of H-CoS$_x$/NF, indicating that incorporating Mo atoms can significantly improve the electrocatalytic activities [43]. According to a previous report [44], the interaction between Mo and Co atoms can change the free energy (ΔG) of certain steps in HER and OER, increasing the electrocatalytic activities. Meanwhile, owing to the high OER activity of NiFe LDH nanosheets, NiFe LDH/NF and H-CMS$_x$@NiFe LDH/NF exhibited lower required overpotentials at all current densities compared with the other catalysts. Correspondingly, H-CMS$_x$@NiFe LDH/NF required the lowest overpotentials of 253, 283, and 299 mV to reach current density of 10, 50, and 100 mA·cm^{-2}, respectively. Furthermore, H-CMS$_x$@NiFe LDH/NF also had the lowest corresponding Tafel slope of 50 mV·dec^{-1}

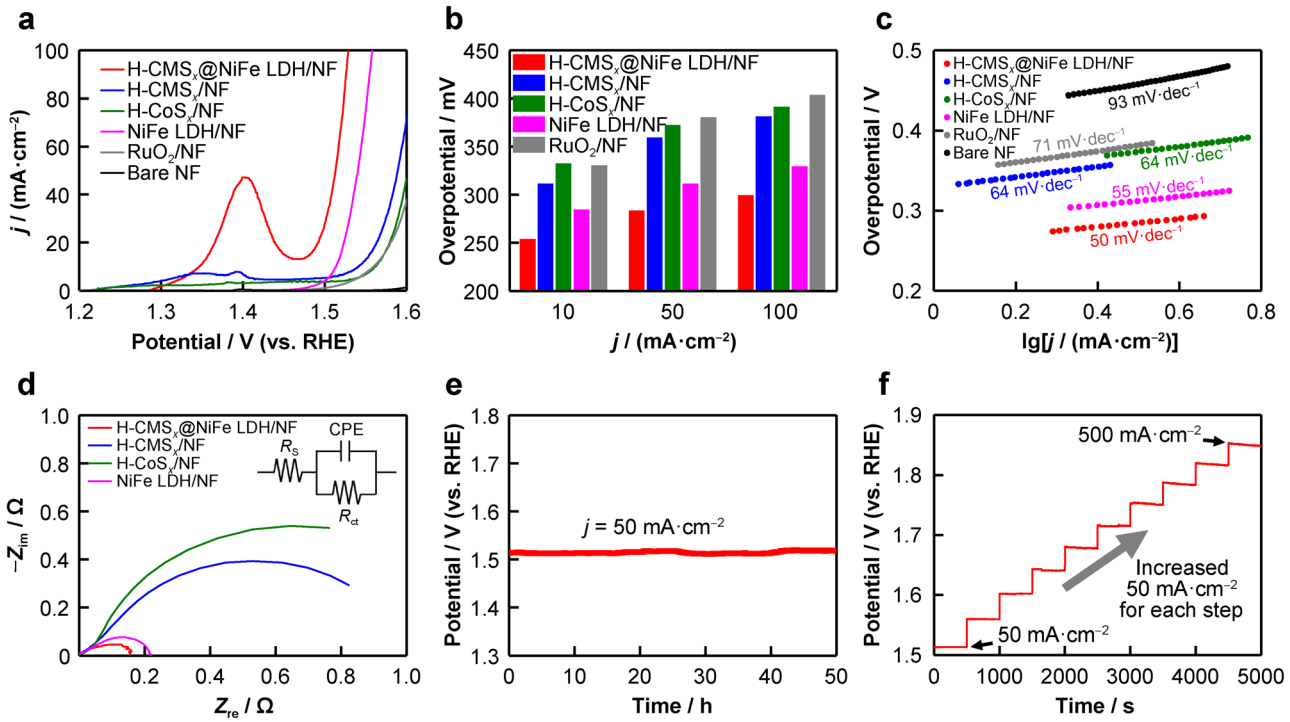

Fig. 4 OER performance data of electrocatalysts: **a** LSV curves measured with a scan rate of 2 mV·s^{-1}; **b** overpotential bar-chart comparison at constant current densities of 10, 50, and 100 mA·cm^{-2}; **c** Tafel plots and **d** Nyquist plots measured at 1.58 (V vs. RHE); **e** stability test of H-CMS$_x$@NiFe LDH/NF at a constant current density of 50 mA·cm^{-2}; **f** multi-step chronopotentiometric curves of H-CMS$_x$@NiFe LDH/NF from 50 to 500 mA·cm^{-2} at intervals of 50 mA·cm^{-2} (every 500 s)

(Fig. 4c), suggesting its faster reaction kinetics [45]. Electrochemical impedance spectroscopy (EIS) analysis was conducted at 1.58 V to further investigate the electron transfer kinetics (Fig. 4d). The diameter of semicircles in the middle-low frequency region of Nyquist plots was related to the charge transfer resistance (R_{ct}) (inset in Fig. 4d) [46]. Thus, the smallest semicircle of H-CMS$_x$@NiFe LDH/NF indicated the fastest charge transfer kinetics at the electrode/electrolyte interface. In the long-term stability test for 50 h at a constant current density of 50 mA·cm^{-2} (Fig. 4e), the potential of H-CMS$_x$@NiFe LDH/NF remained nearly constant with only small degradation of 2.3%. Moreover, in multi-step chronopotentiometric curves of H-CMS$_x$@NiFe LDH/NF, the potential remained stable even at high current densities without significant changes in overpotential, corroborating the excellent stability in OER reaction (Fig. 4f).

Besides superior OER performance, H-CMS$_x$@NiFe LDH/NF showed significant HER activity (Fig. 5). As shown in Fig. 5b, Pt-C/NF exhibited the required overpotentials of 80, 115 and 153 mV at 10, 50 and 100 mA·cm^{-2}, respectively, which are similar to those in previous studies [47]. NiFe LDH/NF showed the lowest HER performance but superior OER performance because of its large energy barrier for the Volmer step [48]. In addition, the required overpotentials to achieve each current density were low in the order of H-CoS$_x$/NF > H-CMS$_x$/NF > H-CMS$_x$@NiFe LDH/NF, which is the same trend as the OER performance; H-CMS$_x$@NiFe LDH/NF exhibited overpotentials of 118, 183 and 214 mV at 10, 50 and 100 mA·cm^{-2}, respectively. Furthermore, the Tafel slope of H-CMS$_x$@NiFe LDH/NF (Fig. 5c) was 90 mV·dec^{-1}, indicating that the H_2 evolution follows the Volmer-Heyrovsky mechanism [49]. In EIS results (Fig. S7), the R_{ct} for H-CMS$_x$@NiFe LDH/NF was much smaller than these of other catalysts, which is favorable to interfacial charge transfer kinetics [50]. In the long-term HER test, the overpotential increased by only 1.6% for 50 h (Fig. 5d). In addition, no significant change in overvoltage was observed when the multi-step chronopotentiometry analysis was performed over various current densities at 500 mA·cm^{-2} increased to 50 for each step (Fig. 5e). To explore the electrochemical surface area of the catalysts, the double-layer capacitance (C_{dl}) values were calculated from the cyclic voltammogram (CV) obtained in the non-faradaic potential region (Fig. S8). The calculated C_{dl} of H-CMS$_x$@NiFe LDH/NF, H-CMS$_x$/NF, H-CoS$_x$/NF, and NiFe LDH/NF were 81.0, 35.9, 27.2, and 2.5 mF·cm^{-2}, respectively (Fig. 5f). The highest C_{dl} value of H-CMS$_x$@NiFe LDH/NF is mostly attributed to the

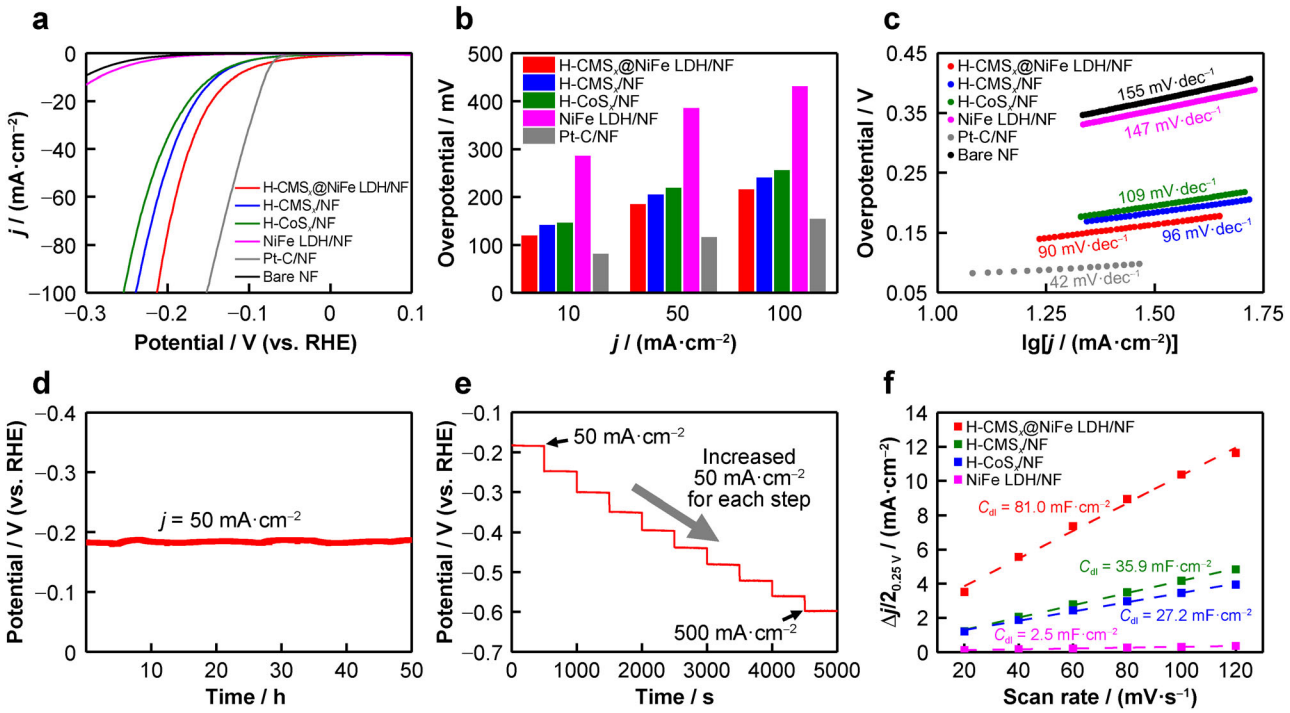

Fig. 5 HER performance data of electrocatalysts: **a** LSV curves measured with a scan rate of 2 mV·s^{-1}; **b** overpotential bar-chart comparison at constant current densities of 10, 50, and 100 mA·cm^2; **c** Tafel plots and **d** stability test of H-CMS$_x$@NiFe LDH/NF at a constant current density of 50 mA·cm^{-2}; **e** multi-step chronopotentiometric curves of H-CMS$_x$@NiFe LDH/NF from 50 to 500 mA·cm^{-2} at intervals of 50 mA·cm^{-2} (every 500 s); **f** double-layer capacitance values calculated from current densities (@0.25 V vs. RHE) *vs.* scan rates

dense loading of ultra-thin NiFe LDH with reduced lateral size on the surface of H-CMS$_x$ nanotriangles, which can present sufficient catalytic active sites for the efficient electrochemical reactions [51, 52]. The OER and HER activities of H-CMS$_x$@NiFe LDH/NF in an alkaline condition were compared to previously reported NF-based electrocatalysts, proving the outstanding electrocatalytic performance of H-CMS$_x$@NiFe LDH/NF (Tables S1, S2).

These superior OER and HER catalytic activities of H-CMS$_x$@NiFe LDH/NF can be associated with the following merits: 1) the local charge distribution regulated by the construction of a heterojunction between H-CMS$_x$ and NiFe LDH can enhance the reaction kinetics; 2) the hollow structure of CMS$_x$ and densely loaded ultra-thin NiFe LDH nanosheets can not only facilitate electrolyte penetration and slippage of gases during the reactions, but also provide more catalytic active sites; 3) the synergistic effect between Co and Mo results in enhanced electrocatalytic activities by the free energy change in both reactions.

Owing to the impressive HER and OER activities of H-CMS$_x$@NiFe LDH/NF, we fabricated a symmetrical electrode cell consisting of H-CMS$_x$@NiFe LDH/NF for water electrolysis (Fig. 6). Figure 6a shows the successful evolution of oxygen and hydrogen gas at the anode (+) and cathode (-) of the fabricated electrolyzer, respectively. As shown in Fig. 6b, c, the H-CMS$_x$@NiFe LDH/NF (+,−) electrolyzer required a much smaller operating potential of 1.60 V to generate the current density of 10 mA·cm^{-2} than H-CMS$_x$/NF(+ ,−) (1.69 V), H-CoS$_x$/NF(+,−) (1.73 V), NiFe LDH/NF(+,−) (1.80 V), and RuO$_2$/NF (+)‖Pt-C/NF (−) (1.64 V). Even to achieve a very high current density of 400 mA·cm^{-2}, the H-CMS·@NiFe LDH/NF electrolyzer required a low operating potential of 1.99 V, which is competitive with previously reported catalysts (Table S3). In Fig. S9, the mass-normalized activity trend of catalysts was similar to the results of geometry area-normalized activity results (Figs. 4a, 5a, 6b); the electrochemical activity of H-CMS$_x$@NiFe LDH/NF in HER, OER and water splitting outperforms that of other samples even in mass normalization. To evaluate the utilization efficiency of electrons participating in the water electrolysis reaction, the Faradaic efficiency (FE) was calculated by measuring the gas volume for 60 min (5 min intervals) at a current density of 50 mA·cm^{-2} (Fig. S10), and it was determined to be ~ 97% (Fig. 6d). The stability test result for the H-CMS$_x$@NiFe LDH/NF (+,−) electrolyzer is shown in Fig. 6e. The operating potential remained stable for 50 h without a significant increase (3.6%),

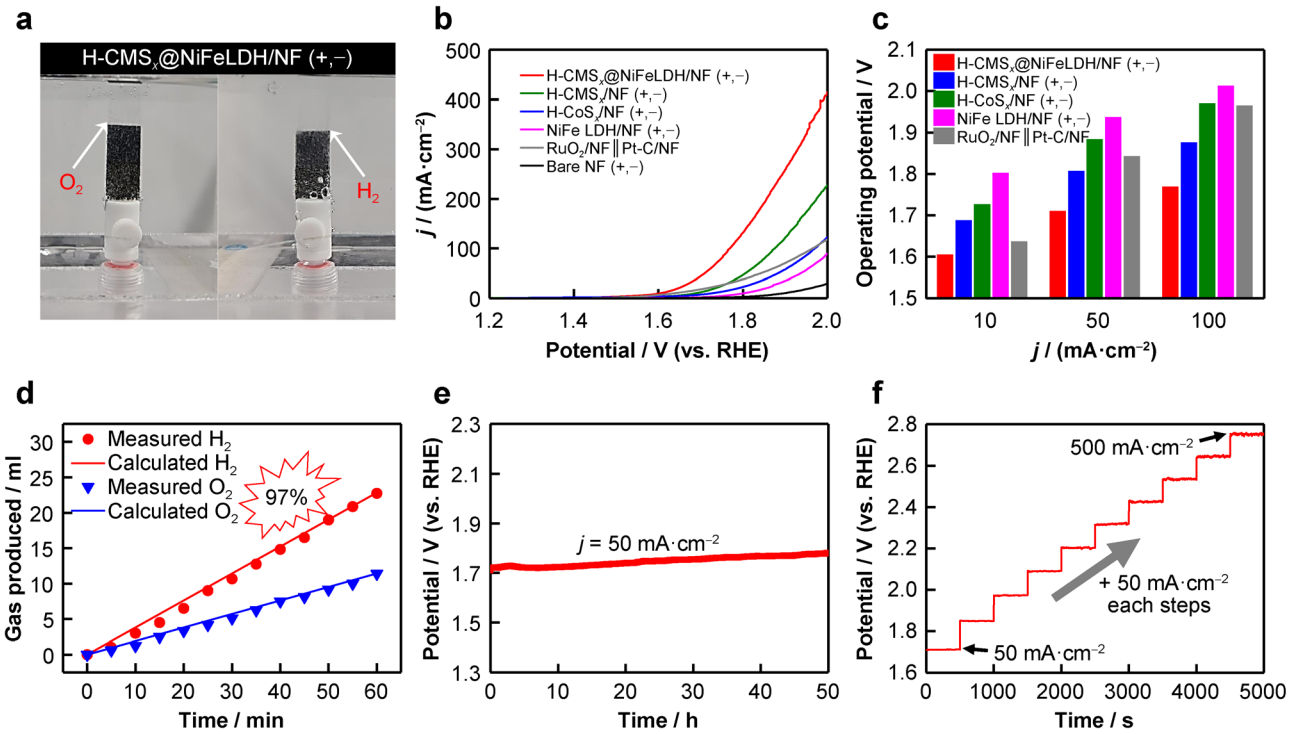

Fig. 6 Overall water splitting activity of H-CMS$_x$@NiFe LDH/NF (+ , −): **a** a photo of O_2 and H_2 generated at the anode and cathode; **b** LSV curves measured at a scan rate of 2 mV·s^{-1}; **c** overpotential bar-chart comparison at constant current densities of 10, 50, and 100 mA·cm^{-2}; **d** volume of experimentally captured H_2 and O_2 production *vs.* theoretically calculated volume under constant current densities of 50 mA·cm^{-2}; **e** long-term stability test of H-CMS$_x$@NiFe LDH/NF (+ , −) at a constant current density of 50 mA·cm^{-2}; **f** the multi-step chronopotentiometric curves of H-CMS$_x$@NiFe LDH/NF from 50 to 500 mA·cm^{-2} at intervals of 50 mA·cm^{-2} (every 500 s)

indicating the excellent durability of the catalysts for water electrolysis. SEM images of H-CMS$_x$@NiFe LDH/NF obtained after the water electrolysis (Fig. S11) showed no considerable structural change of catalysts, verifying the remarkable structural stability. The multi-step Chronopotentiometric curve of the H-CMS$_x$@NiFe LDH/NF electrolyzer further demonstrated the durability of H-CMS$_x$@NiFe LDH/NF for OER and HER reactions.

4 Conclusion

The strong coupled NiFe LDH/CoMoS$_x$ heterojunction hollow nanotriangles were fabricated as highly efficient bifunctional catalysts for overall water splitting. The physicochemical features of the heterostructured catalysts were deeply investigated by various characterization tools. The as-obtained catalysts provide sufficient active sites and facilitate interfacial charge transfer due to the formation of intimate heterojunction interfaces. H-CMS$_x$@NiFe LDH/NF exhibited superior catalytic activities toward HER and OER, with small overpotentials of 214 and 299 mV at 100 mA·cm^{-2}, respectively. In addition, the overall water splitting of H-CMS$_x$@NiFe LDH/NF electrodes exhibited a low operation voltage of 1.99 V to achieve a current density of 400 mA·cm^{-2} with excellent durability of 50 h. The interface engineering and synthetic strategy of the heterostructure can provide new insights into the design of other bifunctional electrocatalysts.

Acknowledgements This work was financially supported by the National Research Foundation of Korea (NRF) from the Korean government (No. 2020R1C1C1003375) and Korea Institute for Advancement of Technology (KIAT) grant funded by the Korea Government (MOTIE) (No. P00124539) (HRD Program for Industrial Innovation).

Declarations

Conflict of interests The authors declare that they have no conflict of interest.

References

[1] Anantharaj S, Ede SR, Sakthikumar K, Karthick K, Mishra S, Kundu S. Recent trends and perspectives in electrochemical water splitting with an emphasis on sulfide, selenide, and phosphide catalysts of Fe Co, and Ni: a review. ACS Catal. 2016;6(12):8069. https://doi.org/10.1021/acscatal.6b02479.

[2] Peng X, Pi C, Zhang X, Li S, Huo K, Chu PK. Recent progress of transition metal nitrides for efficient electrocatalytic water splitting. Sustain Energy Fuels. 2019;3(2):366. https://doi.org/10.1039/C8SE00525G.

[3] Lin J, Yan Y, Li C, Si X, Wang H, Qi J, Cao J, Zhong Z, Fei W, Feng J. Bifunctional electrocatalysts based on Mo-doped NiCoP nanosheet arrays for overall water splitting. Nano-Micro Lett. 2019;11(1):55. https://doi.org/10.1007/s40820-019-0289-6.

[4] Zhang J, Bai X, Wang T, Xiao W, Xi P, Wang J, Gao D, Wang J. Bimetallic nickel cobalt sulfide as efficient electrocatalyst for Zn–air battery and water splitting. Nano-Micro Lett. 2019;11(1):2. https://doi.org/10.1007/s40820-018-0232-2.

[5] Jamesh M-I, Sun X. Recent progress on earth abundant electrocatalysts for oxygen evolution reaction (OER) in alkaline medium to achieve efficient water splitting—a review. J Power Sources. 2018;400:31. https://doi.org/10.1016/j.jpowsour.2018.07.125.

[6] Jiang Y, Lu Y. Designing transition-metal-boride-based electrocatalysts for applications in electrochemical water splitting. Nanoscale. 2020;12(17):9327. https://doi.org/10.1039/D0NR01279C.

[7] Guan S, Fu X, Lao Z, Jin C, Peng Z. NiS–MoS$_2$ hetero--nanosheet array electrocatalysts for efficient overall water splitting. Sustain Energy Fuels. 2019;3(8):2056. https://doi.org/10.1039/C9SE00228F.

[8] Gorlin Y, Jaramillo TF. A bifunctional nonprecious metal catalyst for oxygen reduction and water oxidation. J Am Chem Soc. 2010;132(39):13612. https://doi.org/10.1021/ja104587v.

[9] Li J, Xu W, Luo J, Zhou D, Zhang D, Wei L, Xu P, Yuan D. Synthesis of 3D hexagram-like cobalt–manganese sulfides nanosheets grown on nickel foam: a bifunctional electrocatalyst for overall water splitting. Nano-Micro Lett. 2017;10(1):6. https://doi.org/10.1007/s40820-017-0160-6.

[10] Zhai Z, Li C, Zhang L, Wu H-C, Zhang L, Tang N, Wang W, Gong J. Dimensional construction and morphological tuning of heterogeneous MoS$_2$/NiS electrocatalysts for efficient overall water splitting. J Mater Chem A. 2018;6(21):9833. https://doi.org/10.1039/C8TA03304H.

[11] Hinnemann B, Moses PG, Bonde J, Jørgensen KP, Nielsen JH, Horch S, Chorkendorff I, Nørskov JK. Biomimetic hydrogen evolution: MoS$_2$ nanoparticles as catalyst for hydrogen evolution. J Am Chem Soc. 2005;127(15):5308. https://doi.org/10.1021/ja0504690.

[12] Yu L, Xia BY, Wang X, Lou XW. General formation of M-MoS$_3$ (M = Co, Ni) hollow structures with enhanced electrocatalytic activity for hydrogen evolution. Adv Mater. 2016;28(1):92. https://doi.org/10.1002/adma.201504024.

[13] Staszak-Jirkovský J, Malliakas CD, Lopes PP, Danilovic N, Kota SS, Chang K-C, Genorio B, Strmcnik D, Stamenkovic VR, Kanatzidis MG, Markovic NM. Design of active and stable Co–Mo–S$_x$ chalcogels as pH-universal catalysts for the hydrogen evolution reaction. Nat Mater. 2016;15(2):197. https://doi.org/10.1038/nmat4481.

[14] Dai X, Du K, Li Z, Liu M, Ma Y, Sun H, Zhang X, Yang Y. Co-doped MoS$_2$ nanosheets with the dominant CoMoS phase coated on carbon as an excellent electrocatalyst for hydrogen evolution. ACS Appl Mater Interfaces. 2015;7(49):27242. https://doi.org/10.1021/acsami.5b08420.

[15] Li Y, Yin Z, Cui M, Liu X, Xiong J, Chen S, Ma T. Interface engineering of transitional metal sulfide–MoS$_2$ heterostructure composites as effective electrocatalysts for water-splitting. J Mater Chem A. 2021;9(4):2070. https://doi.org/10.1039/D0TA10815D.

[16] Bao J, Zhou Y, Zhang Y, Sheng X, Wang Y, Liang S, Guo C, Yang W, Zhuang T, Hu Y. Engineering water splitting sites in three-dimensional flower-like Co–Ni–P/MoS$_2$ heterostructural hybrid spheres for accelerating electrocatalytic oxygen and hydrogen evolution. J Mater Chem A. 2020;8(42):22181. https://doi.org/10.1039/D0TA07953G.

[17] Xiong Q, Zhang X, Wang H, Liu G, Wang G, Zhang H, Zhao H. One-step synthesis of cobalt-doped MoS$_2$ nanosheets as bifunctional electrocatalysts for overall water splitting under both acidic and alkaline conditions. Chem Commun. 2018;54(31):3859. https://doi.org/10.1039/C8CC00766G.

[18] Zhang X, Zhou F, Zhang S, Liang Y, Wang R. Engineering MoS_2 basal planes for hydrogen evolution via synergistic ruthenium doping and nanocarbon hybridization. Adv Sci. 2019; 6(10):1900090. https://doi.org/10.1002/advs.201900090.
[19] Zhang B, Liu J, Wang J, Ruan Y, Ji X, Xu K, Chen C, Wan H, Miao L, Jiang J. Interface engineering: the $Ni(OH)_2/MoS_2$ heterostructure for highly efficient alkaline hydrogen evolution. Nano Energy. 2017;37:74. https://doi.org/10.1016/j.nanoen.2017.05.011.
[20] Liu S, Zhang H, Hu E, Zhu T, Zhou C, Huang Y, Ling M, Gao X, Lin Z. Boosting oxygen evolution activity of NiFe-LDH using oxygen vacancies and morphological engineering. J Mater ChemA.2021;9(41):23697.https://doi.org/10.1039/D1TA06263H.
[21] Ren L, Wang C, Li W, Dong R, Sun H, Liu N, Geng B. Heterostructural NiFe-LDH@Ni_3S_2 nanosheet arrays as an efficient electrocatalyst for overall water splitting. Electrochim Acta. 2019;318:42. https://doi.org/10.1016/j.electacta.2019.06.060.
[22] Chen W, Wu B, Wang Y, Zhou W, Li Y, Liu T, Xie C, Xu L, Du S, Song M, Wang D, Liu Y, Li Y, Liu J, Zou Y, Chen R, Chen C, Zheng J, Li Y, Chen J, Wang S. Deciphering the alternating synergy between interlayer Pt single-atom and NiFe layered double hydroxide for overall water splitting. Energy Environ Sci. 2021;14(12):642. https://doi.org/10.1039/D1EE01395E.
[23] Tang Y, Liu Q, Dong L, Wu HB, Yu X-Y. Activating the hydrogen evolution and overall water splitting performance of NiFe LDH by cation doping and plasma reduction. Appl Catal B. 2020;266:118627.https://doi.org/10.1016/j.apcatb.2020.118627.
[24] Wang Q, Shang L, Shi R, Zhang X, Zhao Y, Waterhouse GIN, Wu L-Z, Tung C-H, Zhang T. NiFe layered double hydroxide nanoparticles on Co, N-codoped carbon nanoframes as efficient bifunctional catalysts for rechargeable zinc–air batteries. Adv Energy Mater. 2017;7(21):1700467. https://doi.org/10.1002/aenm.201700467.
[25] Lu X, Xue H, Gong H, Bai M, Tang D, Ma R, Sasaki T. 2D layered double hydroxide nanosheets and their derivatives toward efficient oxygen evolution reaction. Nano-Micro Lett. 2020;12(1):86. https://doi.org/10.1007/s40820-020-00421-5.
[26] Zhang B, Zhu C, Wu Z, Stavitski E, Lui YH, Kim T-H, Liu H, Huang L, Luan X, Zhou L, Jiang K, Huang W, Hu S, Wang H, Francisco JS. Integrating Rh species with NiFe-layered double hydroxide for overall water splitting. Nano Lett. 2020;20(1):136. https://doi.org/10.1021/acs.nanolett.9b03460.
[27] Zhang H, Li X, Hähnel A, Naumann V, Lin C, Azimi S, Schweizer SL, Maijenburg AW, Wehrspohn RB. Bifunctional heterostructure assembly of NiFe LDH nanosheets on NiCoP nanowires for highly efficient and stable overall water splitting. Adv Funct Mater. 2018;28(14):1706847. https://doi.org/10.1002/adfm.201706847.
[28] Feng X, Shi Y, Shi J, Hao L, Hu Z. Superhydrophilic 3D peony flower-like Mo-doped Ni_2S_3@NiFe LDH heterostructure electrocatalyst for accelerating water splitting. Int J Hydrog Energy. 2021;46(7):5169.https://doi.org/10.1016/j.ijhydene.2020.11.018.
[29] Jia Y, Zhang L, Gao G, Chen H, Wang B, Zhou J, Soo MT, Hong M, Yan X, Qian G, Zou J, Du A, Yao X. A heterostructure coupling of exfoliated Ni–Fe hydroxide nanosheet and defective graphene as a bifunctional electrocatalyst for overall water splitting. Adv Mater. 2017;29(17):1700017. https://doi.org/10.1002/adma.201700017.
[30] Zhang X, Qiu Y, Li Q, Liu F, Ji X, Liu J. Facile construction of well-defined hierarchical $NiFe_2O_4$/NiFe layered double hydroxides with a built-in electric field for accelerating water splitting at the high current density. Int J Hydrog Energy. 2022; 47(97):40826. https://doi.org/10.1016/j.ijhydene.2022.09.171.
[31] Liu K-K, Zhang W, Lee Y-H, Lin Y-C, Chang M-T, Su C-Y, Chang C-S, Li H, Shi Y, Zhang H, Lai C-S, Li L-J. Growth of large-area and highly crystalline MoS_2 thin layers on insulating substrates. Nano Lett. 2012;12(3):1538. https://doi.org/10.1021/nl2043612.
[32] Shit S, Bolar S, Murmu NC, Kuila T. Minimal lanthanum-doping triggered enhancement in bifunctional water splitting activity of molybdenum oxide/sulfide heterostructure through structural evolution. Chem Eng J. 2022;428:131131. https://doi.org/10.1016/j.cej.2021.131131.
[33] Hu L, Zeng X, Wei X, Wang H, Wu Y, Gu W, Shi L, Zhu C. Interface engineering for enhancing electrocatalytic oxygen evolution of NiFe LDH/NiTe heterostructures. Appl Catal B. 2020;273:119014. https://doi.org/10.1016/j.apcatb.2020.119014.
[34] Wan C, Jin J, Wei X, Chen S, Zhang Y, Zhu T, Qu H. Inducing the SnO_2-based electron transport layer into NiFe LDH/NF as efficient catalyst for OER and methanol oxidation reaction. J Mater Sci Technol. 2022;124:102. https://doi.org/10.1016/j.jmst.2022.01.022.
[35] Yu J, Liu Z, Yu F, Bao W, Peng B, Wang G, Zhang L, Xu Y, Wang F. Enhanced photoelectrochemical performance of ZnO/NiFe-layered double hydroxide for water splitting: experimental and photo-assisted density functional theory calculations. J Colloid Interface Sci. 2022;623:285. https://doi.org/10.1016/j.jcis.2022.05.001.
[36] Gao R, Yan D. Fast formation of single-unit-cell-thick and defect-rich layered double hydroxide nanosheets with highly enhanced oxygen evolution reaction for water splitting. Nano Res. 2018;11(4):1883. https://doi.org/10.1007/s12274-017-1806-x.
[37] Huang Z, Chen Z, Chen Z, Lv C, Humphrey MG, Zhang C. Cobalt phosphide nanorods as an efficient electrocatalyst for the hydrogen evolution reaction. Nano Energy. 2014;9:373. https://doi.org/10.1016/j.nanoen.2014.08.013.
[38] Wen Q, Yang K, Huang D, Cheng G, Ai X, Liu Y, Fang J, Li H, Yu L, Zhai T. Schottky heterojunction nanosheet array achieving high-current-density oxygen evolution for industrial water splitting electrolyzers. Adv Energy Mater. 2021;11(46): 2102353. https://doi.org/10.1002/aenm.202102353.
[39] Xu R, Wu R, Shi Y, Zhang J, Zhang B. Ni_3Se_2 nanoforest/Ni foam as a hydrophilic, metallic, and self-supported bifunctional electrocatalyst for both H_2 and O_2 generations. Nano Energy. 2016;24:103. https://doi.org/10.1016/j.nanoen.2016.04.006.
[40] Yu L, Yang JF, Guan BY, Lu Y, Lou XWD. Hierarchical hollow nanoprisms based on ultrathin Ni-Fe layered double hydroxide nanosheets with enhanced electrocatalytic activity towards oxygen evolution. Angew Chem Int Ed. 2018;130(1):178. https://doi.org/10.1002/ange.201710877.
[41] Tan L, Yu J, Wang C, Wang H, Liu X, Gao H, Xin L, Liu D, Hou W, Zhan T. Partial sulfidation strategy to NiFe-LDH@Fe-Ni_2S_4 heterostructure enable high-performance water/seawater oxidation. Adv Funct Mater. 2022;32(29):2200951. https://doi.org/10.1002/adfm.202200951.
[42] Gao Z-W, Liu J-Y, Chen X-M, Zheng X-L, Mao J, Liu H, Ma T, Li L, Wang W-C, Du X-W. Engineering NiO/NiFe LDH intersection to bypass scaling relationship for oxygen evolution reaction via dynamic tridimensional adsorption of intermediates. Adv Mater. 2019;31(11):1804769. https://doi.org/10.1002/adma.201804769.
[43] Zhang J, Guo S, Xiao B, Lin Z, Yan L, Du D, Shen S. Ni-Mo based mixed-phase polyionic compounds nanorod arrays on nickel foam as advanced bifunctional electrocatalysts for water splitting. Chem Eng J. 2021;416:129127. https://doi.org/10.1016/j.cej.2021.129127.
[44] Guan C, Xiao W, Wu H, Liu X, Zang W, Zhang H, Ding J, Feng YP, Pennycook SJ, Wang J. Hollow Mo-doped CoP nanoarrays

for efficient overall water splitting. Nano Energy. 2018;48:73. https://doi.org/10.1016/j.nanoen.2018.03.034.
[45] Huang L, Chen D, Luo G, Lu Y-R, Chen C, Zou Y, Dong C-L, Li Y, Wang S. Zirconium-regulation-induced bifunctionality in 3D cobalt–iron oxide nanosheets for overall water splitting. Adv Mater. 2019;31(28):1901439. https://doi.org/10.1002/adma.201901439.
[46] Zhu M, Sun Z, Fujitsuka M, Majima T. Z-scheme photocatalytic water splitting on a 2D heterostructure of black phosphorus/bismuth vanadate using visible light. Angew Chem Int Ed. 2018;57(8):2160. https://doi.org/10.1002/anie.201711357.
[47] Gao Y, Zhang D, Li J, Gong H, Jiang C, Xue H, Huang X, Wang T, He J. The core/shell structure P doped MoS_2@Ni_3S_2 nanorods array for high current density hydrogen evolution in alkaline and acidic electrolyte. Chem Eur J. 2022;28(71):e202202410. https://doi.org/10.1002/chem.202202410.
[48] Li W, Feng B, Yi L, Li J, Hu W. Highly efficient alkaline water splitting with Ru-doped Co−V layered double hydroxide nanosheets as a bifunctional electrocatalyst. Chemsuschem. 2021;14(2):730. https://doi.org/10.1002/cssc.202002509.
[49] Sun H, Zhang W, Li J-G, Li Z, Ao X, Xue K-H, Ostrikov KK, Tang J, Wang C. Rh-engineered ultrathin NiFe-LDH nanosheets enable highly-efficient overall water splitting and urea electrolysis. Appl Catal B. 2021;284:119740. https://doi.org/10.1016/j.apcatb.2020.119740.
[50] Liu Y, Feng Q, Liu W, Li Q, Wang Y, Liu B, Zheng L, Wang W, Huang L, Chen L, Xiong X, Lei Y. Boosting interfacial charge transfer for alkaline hydrogen evolution via rational interior Se modification. Nano Energy. 2021;81:105641. https://doi.org/10.1016/j.nanoen.2020.105641.
[51] Wang B, Jiao S, Wang Z, Lu M, Chen D, Kang Y, Pang G, Feng S. Rational design of NiFe LDH@Ni_3N nano/microsheet arrays as a bifunctional electrocatalyst for overall water splitting. J Mater Chem A. 2020;8(33):17202. https://doi.org/10.1039/D0TA01966F.
[52] Yu L, Zhou H, Sun J, Qin F, Yu F, Bao J, Yu Y, Chen S, Ren Z. Cu nanowires shelled with NiFe layered double hydroxide nanosheets as bifunctional electrocatalysts for overall water splitting. Energy Environ Sci. 2017;10(8):1820. https://doi.org/10.1039/C7EE01571B.